Studies on quark-mass dependence of the $N^*(920)$ pole from unitarized πN χPT amplitudes*

Xu Wang (王旭)[1†] Kai-Ge Kang (康凯歌)[1,2‡] Qu-Zhi Li (李衢智)[2§]
Zhiguang Xiao (肖志广)[2¶] Han-Qing Zheng (郑汉青)[2#]

[1]School of Physics, Peking University, Beijing 100871, China
[2]Institute of Particle and Nuclear Physics, College of Physics, Sichuan University, Chengdu 610065, China

Abstract: The quark-mass dependence of the $N^*(920)$ pole is analyzed using the K-matrix method, with the πN scattering amplitude calculated up to the $O(p^3)$ order in the chiral perturbation theory. As the quark mass increases, the $N^*(920)$ pole gradually approaches the real axis in the complex w-plane (where $w=\sqrt{s}$). Eventually, in the $O(p^2)$ case, it crosses the u-cut on the real axis and enters the adjacent Riemann sheet when the pion mass reaches 526 MeV. At order $O(p^3)$, the rate at which it approaches the real axis decreases; however, it remains uncertain whether it will ultimately cross the u-cut and enter the adjacent Riemann sheet. In addition, the trajectory of the $N^*(920)$ pole is in qualitative agreement with the results from the linear σ model calculation.

Keywords: pion-nucleon scattering, chiral perturbation theory, sub-threshold resonance

DOI: 10.1088/1674-1137/ae4a0b **CSTR:** 32044.14.ChinesePhysicsC.50053108

I. INTRODUCTION

Pion-nucleon scattering has been studied for over six decades; therefore, it is surprising that the pole structure of the sub-threshold $\pi-N$ scattering amplitude, particularly in the S_{11} channel, has only been clarified very recently. Two key findings have emerged: first, as demonstrated in Ref. [1], partial-wave amplitudes (PWAs) indeed contain poles, specifically, virtual states, located on the real axis below threshold on the second Riemann sheet (RSII). Second, a novel resonance pole has been identified in the S_{11} channel through various unitarized approaches, including product representation [2−4], K-matrix fit [5], and N/D method [6]. The resonance pole is necessary because the contribution of the left-hand cut to the phase shift is negative and the pole has to compensate the left-hand cut to reproduce the experimental phase shift [3, 4]. The existence of this resonance has finally been confirmed by the *model-independent* Roy-Steiner equation formalism [7, 8], which respects analyticity, unitarity, and crossing symmetry of the S matrix. This sub-threshold pole located at $\sqrt{s}=(918\pm3)-\mathrm{i}(163\pm9)$ MeV has been designated as $N^*(920)$. See [9, 10] for recent reviews.

Meanwhile, understanding the quark-mass dependence of resonance poles is crucial to gain a unique perspective on strong interaction physics. Lattice quantum chronodynamics (QCD) provides a first-principle, non-perturbative framework to investigate how hadron states depend on quark mass. However, parameterizations of infinite-volume PWAs can introduce model dependence when fitting finite-volume spectra using the Lüscher formula [11] and its generalizations [12−14]. Ref. [15] demonstrated a model-independent approach for interpreting lattice data via the generalized Roy equation, which reveals that the σ meson becomes a bound state, with a new resonance emerging at $m_\pi\simeq391$ MeV. Similar studies have also been completed for πK scattering, as detailed in Refs. [16, 17]. Subsequently, the trajectory of σ with varying m_π was illustrated within the $O(N)$ linear σ model (LσM) [18, 19].

The first attempt to trace the trajectory of the $N^*(920)$ with varying pion masses was conducted within the LσM with nucleons [20]. In that renormalizable model, the au-

Received 12 December 2025; Accepted 25 February 2026; Accepted manuscript online 26 February 2026
* Supported by China National Natural Science Foundation (12335002, 12375078) and the Fundamental Research Funds for the Central Universities
† E-mail: wangxu0604@stu.pku.edu.cn
‡ E-mail: kaige@alumni.pku.edu.cn
§ E-mail: liqz@scu.edu.cn (Corresponding author)
¶ E-mail: xiaozg@scu.edu.cn (Corresponding author)
# E-mail: zhenghq@scu.edu.cn

thors simultaneously computed the trajectories of both the σ and $N^*(920)$ using several unitarization methods at the one-loop level. The trajectory of the σ was found to be consistent with previous results, while that of the $N^*(920)$ was novel: it crossed the u-cut (the cut (c_L, c_R) in Fig. 1) to the adjacent Riemann sheet at tree level, disappearing from the RSII; however, it continued to remain on the complex plane of the RSII at the one-loop level.

To further clarify the fate of $N^*(920)$, this work employs the baryon chiral perturbation theory (BχPT) to investigate its trajectory with increases in pion mass. As a low-energy effective field theory of QCD, BχPT has been successfully applied to describe πN elastic scattering phase shifts and the pion-nucleon σ term. A particular advantage of BχPT in studies with unphysical pion masses is that other parameters such as the nucleon mass m_N, pion decay constant F_π, and axial coupling constant g_A can be determined self-consistently once the low-energy constants are fixed at the physical pion mass. The $\Delta(1232)$ state is not explicitly included because it appears in the P_{33} channel and affects S_{11} only through the crossed channel and higher-order loop effects. Thus, its contributions is expected to be small.

The remainder of this paper is organized as follows: Section II briefly introduces BχPT and PWAs of πN scatterings. In section III, the trajectory of $N^*(920)$ is presented at $O(p^2)$ and $O(p^3)$ orders for different sets of low-energy constant (LEC) values. We conclude with a brief summary in section IV.

II. A BRIEF INTRODUCTION TO BχPT AND PWAs OF πN SCATTERINGS

The Lagrangian in BχPT can be expanded as $\mathcal{L} = \sum_{i=1}^{\infty}\mathcal{L}_{\pi\pi}^{(2i)} + \sum_{j=1}^{\infty}\mathcal{L}_{\pi N}^{(j)}$, where the magnitudes of $\mathcal{L}_{\pi\pi}^{(2i)}$ and $\mathcal{L}_{\pi N}^{(j)}$ are $O(p^{2i})$ and $O(p^j)$, respectively. Terms of the meson part for calculation up to $O(p^4)$ are [21]

$$\mathcal{L}_{\pi\pi}^{(2)} = \frac{F^2}{4}\mathrm{Tr}\left[\nabla_\mu U(\nabla^\mu U)^\dagger\right] + \frac{F^2}{4}\mathrm{Tr}\left[\chi U^\dagger + U\chi^\dagger\right], \tag{1}$$

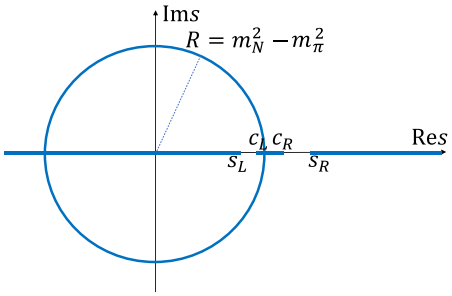

Fig. 1. (color online) Cuts in πN PWAs, represented by the bold lines. $s_L = (m_N - m_\pi)^2$, $c_L = (m_N^2 - m_\pi^2)^2/m_N^2$, $c_R = m_N^2 + 2m_\pi^2$, $s_R = (m_N + m_\pi)^2$.

$$\mathcal{L}_{\pi\pi}^{(4)} = \frac{l_3 + l_4}{16}\left[\mathrm{Tr}\left(\chi U^\dagger + U\chi^\dagger\right)\right]^2 + \frac{l_4}{8}\mathrm{Tr}\left[\nabla_\mu U(\nabla^\mu U)^\dagger\right]\mathrm{Tr}\left(\chi U^\dagger + U\chi^\dagger\right), \tag{2}$$

where F represents the pion decay constant in the chiral limit. $\chi = M^2\mathbb{1}$ (assuming isospin symmetry) and M represents the lowest-order pion mass. Pions are contained in the $SU(2)$ matrix.

$$U = \exp\left(\mathrm{i}\frac{\phi}{F}\right), \quad \phi = \vec{\phi}\cdot\vec{\tau} = \begin{pmatrix} \pi_0 & \sqrt{2}\pi^+ \\ \sqrt{2}\pi^- & -\pi_0 \end{pmatrix}, \tag{3}$$

The covariant derivative acting on the pion fields is defined as $\nabla_\mu U = \partial_\mu U - \mathrm{i}r_\mu U + \mathrm{i}Ul_\mu$, where l_μ and r_μ are the external fields.

The required baryon Lagrangians for calculation up to $O(p^3)$ are [22]

$$\mathcal{L}_{\pi N}^{(1)} = \overline{\Psi}\left\{\mathrm{i}\not{D} - m + \frac{g}{2}\not{\gamma}\gamma_5 u_\mu\right\}\Psi, \tag{4}$$

$$\mathcal{L}_{\pi N}^{(2)} = \overline{\Psi}\left\{c_1\mathrm{Tr}[\chi_+] - \frac{c_2}{4m^2}\mathrm{Tr}[u_\mu u_\mu](D^\mu D^\mu + \mathrm{h.c.}) + \frac{c_3}{2}\mathrm{Tr}[u^\mu u_\mu] - \frac{c_4}{4}\not{\gamma}\not{\gamma}[u_\mu, u_u]\right\}\Psi, \tag{5}$$

$$\begin{aligned}\mathcal{L}_{\pi N}^{(3)} = \overline{\Psi}\Bigg\{ & -\frac{d_1 + d_2}{4m}\left([u_\mu, [D_u, u^\mu] + [D^\mu, u_u]]D^\mu + \mathrm{h.c.}\right) \\ & + \frac{d_3}{12m^3}\left([u_\mu, [D_u, u_\lambda]]\left(D^\mu D^u D^\lambda + \mathrm{sym.}\right) + \mathrm{h.c.}\right) \\ & + \mathrm{i}\frac{d_5}{2m}\left([\chi_-, u_\mu]D^\mu + \mathrm{h.c.}\right) \\ & + \mathrm{i}\frac{d_{14} - d_{15}}{8m}\left(\sigma^{\mu u}\mathrm{Tr}\left[[D_\lambda, u_\mu]u_u - u_\mu[D_u, u_\lambda]\right]D^\lambda + \mathrm{h.c.}\right) \\ & + \frac{d_{16}}{2}\not{\gamma}\not{\gamma}\mathrm{Tr}\left[\chi_+\right]u_\mu + \frac{\mathrm{i}d_{18}}{2}\not{\gamma}\not{\gamma}\left[D_\mu, \chi_-\right]\Bigg\}\Psi,\end{aligned} \tag{6}$$

where m and g represent the bare nucleon mass and bare axial-vector coupling constant, respectively. Parameters l_i, c_i, and d_i are the LECs. The chiral vielbein and the covariant derivative with respect to the nucleon field are defined as

$$u_\mu = \mathrm{i}\left[u^\dagger\left(\partial_\mu - \mathrm{i}r_\mu\right)u - u\left(\partial_\mu - \mathrm{i}l_\mu\right)u^\dagger\right], \tag{7}$$

$$D_\mu = \partial_\mu + \Gamma_\mu, \tag{8}$$

$$\Gamma_\mu = \frac{1}{2}\left[u^\dagger\left(\partial_\mu - \mathrm{i}r_\mu\right)u + u\left(\partial_\mu - \mathrm{i}l_\mu\right)u^\dagger\right], \tag{9}$$

$$u = \sqrt{U} = \exp\left(\frac{\mathrm{i}\phi}{2F}\right). \tag{10}$$

According to the power counting rule [23], the order of the amplitude for a diagram with L loops, I_ϕ inner pion lines, I_N inner nucleon lines and $N^{(k)}$ vertices from $O(p^k)$ Lagrangian is given as

$$D = 4L - 2I_\phi - I_N + \sum_k^\infty kN^{(k)}.$$

In this work, the full amplitudes of πN scatterings are calculated up to the $O(p^3)$ order.

For the process $\pi^a(p) + N_i(q) \to \pi^{a'}(p') + N_f(q')$, the isospin amplitude can be decomposed as

$$T = \chi_f^\dagger\left(\delta^{aa'}T^+ + \frac{1}{2}\left[\tau^{a'},\tau^a\right]T^-\right)\chi_i, \tag{11}$$

where τ^a $(a = 1,2,3)$ are Pauli matrices, and χ_i (χ_f) corresponds to the isospin wave function of the initial (final) nucleon state. The amplitudes with isospins $I = 1/2, 3/2$ can be written as

$$T^{I=1/2} = T^+ + 2T^-, \quad T^{I=3/2} = T^+ - T^-. \tag{12}$$

For Lorentz structure with an isospin index $I = 1/2, 3/2$,

$$T^I = \bar{u}^{(s')}(q')\left[A^I(s,t) + \frac{1}{2}\left(\not{p} + \not{p}'\right)B^I(s,t)\right]u^{(s)}(q), \tag{13}$$

with the superscripts $(s),(s')$ denoting the spins of Dirac spinors and three Mandelstam variables $s = (p+q)^2$, $t = (p-p'), u = (p-q')$ obeying the constraint $s+t+u = 2m_N^2 + 2m_\pi^2$. The partial wave amplitude $T_\pm^{I,J}$ for the L_{2I2J} channel with orbital angular momentum L, total angular momentum J, and total isospin I is defined as

$$T_\pm^{I,J} = T(L_{2I2J}) = T_{++}^{I,J}(s) \pm T_{+-}^{I,J}(s), \quad L = J \mp \frac{1}{2}, \tag{14}$$

where the definition of the partial wave helicity amplitudes are written as

$$\begin{aligned} T_{++}^{I,J} &= 2m_N A_C^{I,J}(s) + \left(s - m_\pi^2 - m_N^2\right)B_C^{I,J}(s) \\ T_{+-}^{I,J} &= -\frac{1}{\sqrt{s}}\Big[\left(s - m_\pi^2 + m_N^2\right)A_S^{I,J}(s) \\ &\quad + m_N\left(s + m_\pi^2 - m_N^2\right)B_S^{I,J}(s)\Big] \end{aligned} \tag{15}$$

with

$$F_{C/S}^{I,J}(s) = \int_{-1}^{1} \mathrm{d}z_s F^I(s,t)\left[P_{J+1/2}(z_s) \pm P_{J-1/2}(z_s)\right], \quad F = A, B \tag{16}$$

and $z_s = \cos\theta$ with θ as the scattering angle. The partial wave amplitudes $T_\pm^{I,J}$ satisfy the unitarity condition

$$\mathrm{Im}\, T_\pm^{I,J}(s) = \rho(s, m_\pi, m_N)|T_\pm^{I,J}(s)|^2, \quad s > s_R = (m_\pi + m_N)^2. \tag{17}$$

For simplicity, we denote the PWA $T(S_{11})$ as T in the following.

The partial wave S matrix element in S_{11} channel can be defined as

$$S = 1 + 2\mathrm{i}\rho(s)T, \tag{18}$$

where $\rho(s) = \sqrt{[s-(m_N+m_\pi)^2][s-(m_N-m_\pi)^2]}/s$. A K-matrix approximation is used to restore unitarity from perturbation amplitudes. Then, the partial wave amplitude and partial wave S matrix element are expressed as

$$\tilde{T} = \frac{K}{1 - \mathrm{i}\rho K}, \quad \tilde{S} = \frac{1 + \mathrm{i}\rho K}{1 - \mathrm{i}\rho K}, \tag{19}$$

where K needs to be real in the physical region above the πN threshold to meet the unitary requirement of the S matrix. Typically, K is considered as the real part of the perturbation amplitude. For πN scattering, it is

$$\mathcal{K}^{(2)} \equiv T^{(2)} \tag{20}$$

for the $O(p^2)$ calculation, while $\mathcal{K}^{(3)}$ is set to

$$T^{(3)} - \mathrm{i}\rho(T^{(1)})^2 \tag{21}$$

for the $O(p^3)$ calculation because $T^{(3)}$ contains an imaginary part on the right-hand cut [24].

The partial wave amplitude as constructed is a real analytic function on the complex s plane. There exists a physical cut, or right-hand cut, above the threshold $s > (m_N + m_\pi)^2$. Partial wave projection and loop integrals also introduce other cuts, called left-hand cuts. All the cut structures in πN scattering are shown in Fig. 1 [25, 26]. However, in general, such unitarization approximations suffer from problems of violation of analyticity and crossing symmetry [27–30].[1)] A direct consequence is the appearance of spurious physical sheet resonances (SPSRs). A case by case analysis seems to be required, at least, to ensure that the SPSRs play a minor contribution

1) For example, a [1,1] Padé approximant of $\pi\pi$ scattering tend to put all contributions from different sources, e.g., s channel poles, left hand cuts, crossed channel resonance exchanges, into one single s channel resonance.

to physical quantities such as phase shifts. Barring for this, the K-matrix unitarization provides a quick but rough estimates of the physical pole position such as $N^*(920)$.

III. ANALYSIS OF THE $N^*(920)$ POLE TRAJECTORY AND ITS QUARK MASS DEPENDENCE

To proceed, we follow Refs. [3, 24]. First, we repeat the $O(p^2)$ and $O(p^3)$ results of Ref. [24]. The obtained partial wave unitary amplitude is then used to calculate the corresponding phase shift $\delta = \arctan[\rho\tilde{T}]$. A subsequent fit to the phase shift data determines the LECs. For the $O(p^2)$ calculations, we directly use the results in Ref. [3].

$$c_1 = -0.841\ \text{GeV}^{-1},\ \ c_2 = 1.170\ \text{GeV}^{-1},$$
$$c_3 = -2.618\ \text{GeV}^{-1},\ \ c_4 = 1.677\ \text{GeV}^{-1}\ . \tag{22}$$

By substituting these low energy constants and physical quantities $m_N = 0.9383$ GeV, $m_\pi = 0.1396$ GeV, $F_\pi = 0.0924$ GeV, $g_A = 1.267$, we can calculate the cuts and poles of the partial wave unitary matrix element of the S_{11} channel on the complex s plane. The pole corresponding to $N^*(920)$ resonance is found at $\sqrt{s} = 0.954 \pm$ i0.265 GeV.

In the isospin limit, the pion mass is related to the quark mass by the relation $m_\pi^2 \propto 2B_0\hat{m}$, where $\hat{m} = (m_u + m_d)/2$ [31]. Consequently, investigating the quark-mass dependence of the $N^*(920)$ resonance is equivalent to studying its evolution with increasing pion mass. By definition, the effective Lagrangian is an expansion with respect to m_π and soft momentum p; therefore, the LECs l_i and d_i are m_π independent. The renormalization scheme is selected to be m_π independent, and thus, the renormalized LECs are independent of m_π. In addition, key physical quantities (e.g., m_N, g_A, and F_π) are renormalized; therefore, it is essential to determine their values at different pion masses. Fortunately, within the framework of BχPT, these dependence relations can be directly computed. Up to the $O(p^3)$ order (one-loop diagrams), the explicit dependence relations are given by (this result can also be found in [32–34])

$$\begin{aligned}
&m_N = m - 4c_1M^2 + \Delta_m, \quad \Delta_m = \frac{3g^2 m_N}{32\pi^2 F^2}\left[A_0(m_N^2) + M^2 B_0(m_N^2, M^2, m_N^2)\right],\\
&F_\pi = F\left(1 + l_4^r\frac{M^2}{F^2} - \frac{1}{16\pi^2}\ln\left[\frac{M^2}{\mu^2}\right]\frac{M^2}{F^2}\right), \quad l_4 = l_4^r + \gamma_4\lambda, \quad l_4^r = \frac{\gamma_4}{32\pi^2}\left(\bar{l}_4 + \ln\frac{M^2}{\mu^2}\right), \quad \gamma_4 = 2,\\
&g_A = g + 4d_{16}M^2 + \Delta_g,\\
&\Delta_g = \frac{g\left[4(g^2-2)m_N^2 + (3g^2+2)M^2\right]}{16\pi^2F^2(4m_N^2 - M^2)}A_0[m_N^2] + \frac{g\left[(8g^2+4)m_N^2 - (4g^2+1)M^2\right]}{16\pi^2F^2(4m_N^2 - M^2)}A_0[M^2]\\
&\quad + \frac{gM^2\left[-8(g^2+1)m_N^2 + (3g^2+2)M^2\right]}{16\pi^2F^2(4m_N^2 - M^2)}B_0[m_N^2, m_N^2, M^2] - \frac{g^3 m_N^2(4m_N^2 + 3M^2)}{16\pi^2F^2(4m_N^2 - M^2)},
\end{aligned} \tag{23}$$

where μ represents the renormalization scale which we fix at $\mu = m_N$, and λ represents a m_π independent infinite renormalization constant [21]. The Passarino-Veltman functions, A_0 and B_0, are adopted from [35] and have the analytic expressions

$$A_0[m^2] = m^2\left(-R_\epsilon + \ln\frac{\mu^2}{m^2}\right),$$

$$\begin{aligned}
B_0[p^2, m_1^2, m_2^2] &= 1 - R_\epsilon + \ln\left(\frac{\mu^2}{m_2^2}\right)\\
&+ \frac{1}{2p^2}\left\{\left[p^2(1+\rho) - R_m\right]\ln\left[\frac{R_m + p^2(1-\rho)}{R_m - \rho^2(1+\rho)}\right]\right.\\
&\left. + \left[\rho^2(1-\rho) - R_m\right]\ln\left[\frac{R_m + p^2(1+\rho)}{R_m - \rho^2(1-\rho)}\right]\right\},
\end{aligned} \tag{24}$$

where $R_\epsilon = -\frac{1}{\epsilon} + \gamma_E - \ln(4\pi) - 1$, with $\gamma_E = -\Gamma'(1)$ denoting the Euler constant. ρ and R_m are defined as

$$\rho = \frac{\sqrt{p^2 - (m_1+m_2)^2}\sqrt{p^2 - (m_1-m_2)^2}}{p^2}, \quad R_m = m_2^2 - m_1^2. \tag{25}$$

Using the aforementioned formulas, the resulting dependence relations are visualized in Fig. 2. The following parameter values are adopted in the calculations: $d_{16} = -0.83\,\text{GeV}^{-2}$ [34, 36] and LEC $l_4^r = 0.00373$ is derived through the evolution of its conventional value at the renormalization scale $\mu = 0.77$ [37–38] to $\mu = m_N$. For the three sets of m_N vs. m_π dependence curves presented in Fig. 2, the corresponding c_1 parameters are selected from Ref. [3] for the $O(p^2)$ order, Ref. [39] for the

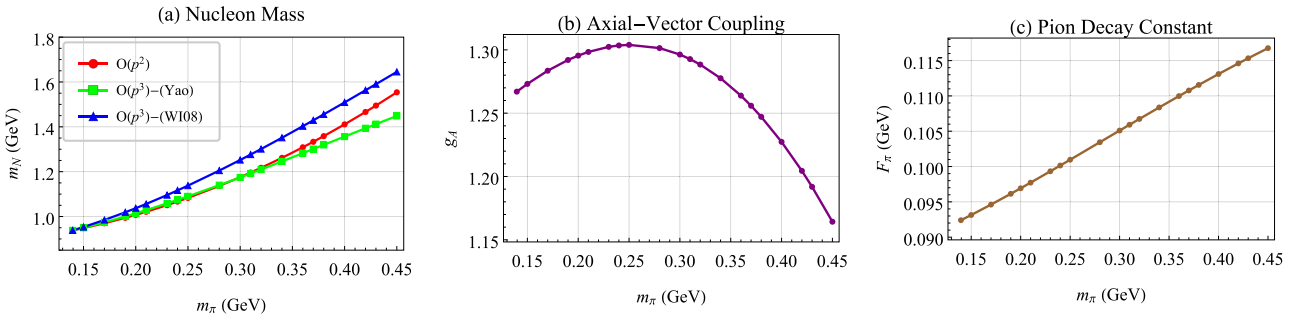

Fig. 2. (color online) Dependencies of the nucleon mass m_N, axial-vector coupling g_A, and pion decay constant F_π on the pion mass m_π.

$O(p^3)-$(Yao) set, and Ref. [40–41] for the $O(p^3)-$(WI08) set. We do not consider explicit $\Delta(1232)$ in the BχPT; therefore, we select the parameter sets in the cases without explicit $\Delta(1232)$ from these references.

By substituting these derived dependence relations into the partial-wave unitary matrix element, we obtain the trajectory of the $N^*(920)$ resonance as pion mass varies from 0.1396 GeV to 0.45 GeV, which is further extended to 0.60 GeV when considering $O(p^2)$ contributions because the $O(p^2)$ calculation is numerically more stable. Fig. 3 illustrates the evolution of this $N^*(920)$ pole trajectory in the w-plane (where $w=\sqrt{s}$): as pion mass increases, the pole gradually migrates toward the real axis. The $O(p^2)$ result shows a more complete picture: the pole ultimately traverses the u-cut (at $m_\pi = 0.526$ GeV), entering the adjacent Riemann sheet. Furthermore, the crossing position is consistent with the result calculated via Equation (43) in Ref. [20], which is expressed as

$$(m_N-m_\pi-w)(m_N+m_\pi-w)\left[m_N(m_N-w)(m_N+w)^2-m_\pi^4\right]=0,$$
$$w=\sqrt{s} \tag{26}$$

For the $O(p^3)$ calculations, more LECs are required compared to that required for $O(p^2)$. We use the results of Fit 1 in Ref. [39](denoted as $O(p^3)-$Yao in Fig. 3).

$$\begin{aligned}
&c_1=-1.22\,\text{GeV}^{-1}, \quad c_2=3.58\,\text{GeV}^{-1},\\
&c_3=-6.04\,\text{GeV}^{-1}, \quad c_4=3.48\,\text{GeV}^{-1}\\
&d_1+d_2=3.25\,\text{GeV}^{-2}, \quad d_3=-2.88\,\text{GeV}^{-2},\\
&d_5=-0.15\,\text{GeV}^{-2}, \quad d_{14}-d_{15}=-6.19\,\text{GeV}^{-2},\\
&d_{18}=-0.47\,\text{GeV}^{-2}
\end{aligned} \tag{27}$$

Using these LECs, the corresponding positions of $N^*(920)$ pole are found to be $\sqrt{s}=0.896\pm i0.258$ GeV. Specifically, as the pion mass increases from 0.1396 GeV to 0.45 GeV, the trajectory of $N^*(920)$ approaches the u-cut, as shown in Fig. 3. We do not track the trajectory for higher m_π to verify if it crosses the u-cut because of three reasons: (1) trajectory evolution is too slow in the loop calculations; (2) the fluctuation in the numerical integral calculation becomes significant, and the searches for the pole become difficult and unstable as the pole approaches the real axis; and (3) since χPT is a perturbative expansion with respect to m_π, it is reasonable to expect that at higher orders the region where it provides a good approximation would become smaller. Thus, the $O(p^3)$ result does not indicate if the pole will touch the u-cut and move across to the adjacent Riemann sheet for larger m_π.

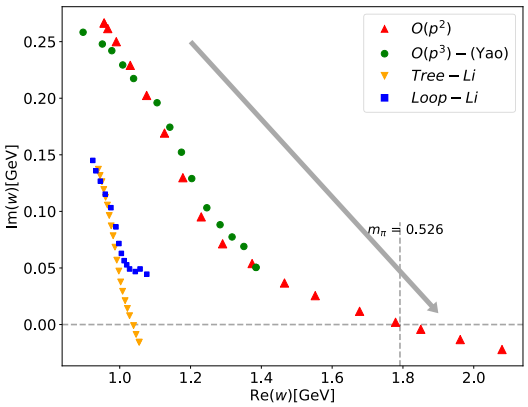

Fig. 3. (color online) Variation of the $N^*(920)$ pole position with the pion mass in the $\mathcal{K}^{(2)}$ and $\mathcal{K}^{(3)}$ amplitudes. The units for the pole positions are in GeV. The results obtained in this work are shown in red upright triangles ($O(p^2)$ tree-level), covering $m_\pi = 0.1396 \sim 0.60$ GeV and green solid circle ($O(p^3)$ one-loop), covering $m_\pi = 0.1396 \sim 0.45$ GeV. The results from Ref. [20] are also displayed in orange upside-down triangles (Tree–Li) and blue squares (Loop–Li), covering the range $m_\pi = 0.138 \sim 0.360$ GeV.

Further, we compare our results with those from Ref. [20], which were obtained using LσM with nucleons. While the overall trends of the trajectories are consistent, the rate at which the pole approaches the real axis in LσM is notably higher at both tree and one-loop levels. This causes the pole to cross the u-cut at a smaller pion mass

in their tree-level calculation. In addition, the authors did not extend their one-loop calculation to very large pion masses because of the limited applicability range of LσM. Consequently, the pole in LσM appears to remain on the complex plane without reaching the real axis. In contrast, in this study, the $O(p^3)$ result shows that the trajectory continues to bend downward toward the real axis with increasing m_π, following a trend similar to the tree-level behavior.

In addition, we tested another set of parameters [40–41], referred to as the WI08 parameter set, and found that the $O(p^3)$ calculation yields consistent results. The results are shown in Fig. 4 below, and the specific parameters are

$$\begin{aligned} &c_1 = -1.50\,\text{GeV}^{-1}, \quad c_2 = 3.76\,\text{GeV}^{-1}, \\ &c_3 = -6.63\,\text{GeV}^{-1}, \quad c_4 = 3.68\,\text{GeV}^{-1} \\ &d_1 + d_2 = 3.67\,\text{GeV}^{-2}, \quad d_3 = -2.63\,\text{GeV}^{-2}, \\ &d_5 = -0.07\,\text{GeV}^{-2}, \quad d_{14} - d_{15} = -6.80\,\text{GeV}^{-2}, \\ &d_{18} = -0.50\,\text{GeV}^{-2}. \end{aligned} \tag{28}$$

In addition to the dependence relations for m_N, g_A, and F_π derived from the chiral perturbation theory, similar results are also obtained by some theoretical fits performed on the lattice data. For m_N, we use the ruler approximation in Ref. [42], that is, $m_N = 800\,\text{MeV} + m_\pi$, which is consistent with the lattice QCD results [43–44] in a large range. For g_A, we use the $O(p^3)$ result in Ref. [45] (Fig. 4.), and for F_π, we use the fit result with strategy 2 (left subfigure in Fig. 4.) in Ref. [46]. Based on these dependence relations, the resulting trajectory of the $N^*(920)$ pole is shown in Fig. 5. The points where the $N^*(920)$ pole approaches the u-cut from the $O(p^2)$ and $O(p^3)$ chiral perturbation theory calculations tend to converge. There is no guarantee that the pole reaches the u-cut at the same m_π for both $O(p^2)$ and $O(p^3)$ results; therefore, this convergence may just be accidental.

As illustrated in this section, the $N^*(920)$ pole trajectory obtained in different approximations and parameter sets are in qualitative agreement with each other.

IV. SUMMARY

In this study, we investigated the trajectory of $N^*(920)$ as the pion mass increases within the BχPT framework both at $O(p^2)$ and $O(p^3)$ orders. In BχPT, the functions of the nucleon mass, pion decay constant, and πN axial-vector coupling as a function of the pion mass are obtained self-consistently, provided that the LECs are fixed. In both cases, the $N^*(920)$ moves along a rightward-downward trajectory toward the u-cut on the complex energy plane. At the$O(p^2)$ level, the pole eventually

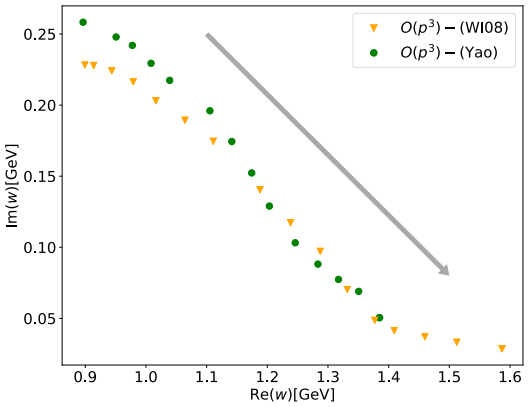

Fig. 4. (color online) m_π dependence of $N^*(920)$ pole from the full $O(p^3)$ amplitude including loop corrections, using parameters from Eq. (31). The previous $O(p^3)$-(Yao) result in Fig. 3 is displayed for comparison.

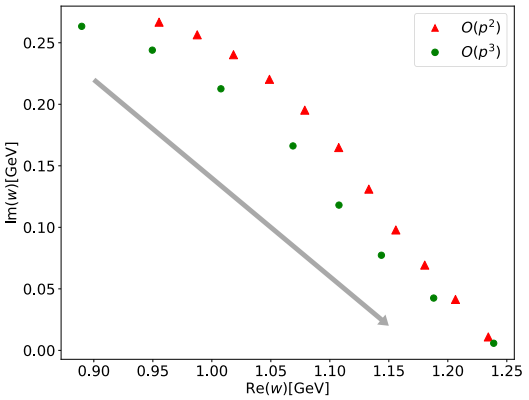

Fig. 5. (color online) Dependence of the $N^*(920)$ pole position on pion mass, as determined from the $\mathcal{K}^{(2)}$ and $\mathcal{K}^{(3)}$ amplitudes (with the dependencies of m_N, g_A, and F_π on m_π taken from lattice–data–based fits). The unit is GeV. The $\mathcal{K}^{(2)}$ results are indicated by red triangles, while the $\mathcal{K}^{(3)}$ results are shown as green circles. The pion mass m_π varies from 0.1396 to 0.44 GeV.

crosses the u-cut, entering the adjacent Riemann sheet defined by the u-cut. The result at the $O(p^3)$ order shows that the circular cut has marginal effects on the trajectory, and the higher-order contributions slow down the approaching rate of the pole. Furthermore, to test the robustness, we employed three different LEC parameter sets. All three results demonstrate that the $N^*(920)$ moves toward the u-cut. However, we cannot confirm if it will meet the u-cut and move across to the adjacent Riemann sheet because the numerical results at $O(p^3)$ become unstable as the pole moves closer to the real axis and the higher order chiral expansion may not be good at larger m_π. Further, the trajectory is compared with the result in the previous work [20], showing qualitatively consistent behaviors. Our analyses in this study may provide valu-

able insights for future Lattice studies with unphysical pion masses.

ACKNOWLEDGMENT

We thank Zhi-Hui Guo for the helpful discussions.

References

[1] Q. Z. Li and H. Q. Zheng, Commun. Theor. Phys. **74**(11), 115203 (2022), arXiv: 2108.03734[nucl-th]
[2] H. Q. Zheng, Z. Y. Zhou, G. Y. Qin *et al.*, Nucl. Phys. A **733**, 235 (2004), arXiv: hep-ph/0310293
[3] Y. F. Wang, D. L. Yao, and H. Q. Zheng, Eur. Phys. J. C **78**(7), 543 (2018), arXiv: 1712.09257[hep-ph]
[4] Y. F. Wang, D. L. Yao, and H. Q. Zheng, Chin. Phys. C **43**(6), 064110 (2019), arXiv: 1811.09748[hep-ph]
[5] Y. Ma, W. Q. Niu, Y. F. Wang *et al.*, Commun. Theor. Phys. **72**(10), 105203 (2020), arXiv: 2002.02351[hep-ph]
[6] Q. Z. Li, Y. Ma, W. Q. Niu *et al.*, Chin. Phys. C **46**(2), 023104 (2022), arXiv: 2102.00977[nucl-th]
[7] X. H. Cao, Q. Z. Li, and H. Q. Zheng, JHEP **12**, 073 (2022), arXiv: 2207.09743[hep-ph]
[8] M. Hoferichter, J. R. de Elvira, B. Kubis *et al.*, Phys. Lett. B **853**, 138698 (2024), arXiv: 2312.15015[hep-ph]
[9] M. Döring, J. Haidenbauer, M. Mai *et al.*, Prog. Part. Nucl. Phys. **146**, 104213 (2026), arXiv: 2505.02745[nucl-th]
[10] Q. Z. Li, Z. Xiao, and H. Q. Zheng, Eur. Phys. J. Spec. Top. (5, 2025), arXiv: 2505.24674 [hep-ph]
[11] M. Luscher, Nucl. Phys. B **354**, 531 (1991)
[12] K. Rummukainen and S. A. Gottlieb, Nucl. Phys. B **450**, 397 (1995), arXiv: hep-lat/9503028
[13] Z. Fu, Phys. Rev. D **85**, 014506 (2012), arXiv: 1110.0319[hep-lat]
[14] L. Leskovec and S. Prelovsek, Phys. Rev. D **85**, 114507 (2012), arXiv: 1202.2145[hep-lat]
[15] X. H. Cao, Q. Z. Li, Z. H. Guo *et al.*, Phys. Rev. D **108**(3), 034009 (2023), arXiv: 2303.02596[hep-ph]
[16] X. H. Cao, F. K. Guo, Z. H. Guo *et al.*, Phys. Rev. D **112**, L031503 (2025), arXiv: 2412.03374[hep-ph]
[17] X. H. Cao, F. K. Guo, Z. H. Guo *et al.*, Phys. Rev. D **112**(3), 034042 (2025), arXiv: 2506.10619[hep-ph]
[18] Y. L. Lyu, Q. Z. Li, Z. Xiao *et al.*, Phys. Rev. D **110**(9), 094054 (2024), arXiv: 2405.11313[hep-ph]
[19] Y. L. Lyu, Q. Z. Li, Z. Xiao *et al.*, Phys. Rev. D **109**(9), 094026 (2024), arXiv: 2402.19243[hep-ph]
[20] Q. Z. Li, Z. Xiao, and H. Q. Zheng, Chin. Phys. C **49**(12), 123103 (2025), arXiv: 2501.01619[hep-ph]
[21] J. Gasser and H. Leutwyler, Annals Phys. **158**, 142 (1984)
[22] N. Fettes, U. G. Meißner, M. Mojžiš, and S. Steininger, Annals Phys. **283**(2), 273 (2000).
[23] S. Weinberg, Nucl. Phys. B **363**(1), 3 (1991)
[24] Y. H. Chen, D. L. Yao, and H. Q. Zheng, Phys. Rev. D **87**, 054019 (2013), arXiv: 1212.1893[hep-ph]
[25] S. W. MacDowell, Phys. Rev. **116**, 774 (1959)
[26] J. Kennedy and T. D. Spearman, Phys. Rev. **126**(4), 1596 (1962)
[27] G. Y. Qin, W. Z. Deng, Z. Xiao *et al.*, Phys. Lett. B **542**, 89 (2002), arXiv: hep-ph/0205214
[28] Z. H. Guo, J. J. Sanz Cillero, and H. Q. Zheng, JHEP **06**, 030 (2007), arXiv: hep-ph/0701232
[29] Z. H. Guo, J. J. Sanz-Cillero, and H. Q. Zheng, Phys. Lett. B **661**, 342 (2008), arXiv: 0710.2163[hep-ph]
[30] D. L. Yao, L. Y. Dai, H. Q. Zheng *et al.*, Rept. Prog. Phys. **84**(7), 076201 (2021), arXiv: 2009.13495[hep-ph]
[31] M. Gell-Mann, R. J. Oakes, and B. Renner, Phys. Rev. **175**, 2195 (1968)
[32] J. Gasser, M. Sainio, and A. Švarc, Nucl. Phys. B **307**(4), 779 (1988)
[33] X. L. Gao, Z. H. Guo, Z. Xiao *et al.*, Phys. Rev. D **105**(9), 094002 (2022), arXiv: 2202.03124[hep-ph]
[34] D. L. Yao, L. Alvarez-Ruso, and M. J. Vicente-Vacas, Physical Review D **96**(11), 116022 (2017)
[35] G. Passarino and M. J. G. Veltman, Nucl. Phys. B **160**, 151 (1979)
[36] J. M. Chen, Z. R. Liang, and D. L. Yao, Front. Phys. (Beijing) **19**(6), 64202 (2024), arXiv: 2403.17743[hep-ph]
[37] J. Bijnens, PoS **CD12**, 002 (2013), arXiv: 1301.6953[hep-ph]
[38] G. Colangelo, J. Gasser, and H. Leutwyler, Nucl. Phys. B **603**(1-2), 125 (2001)
[39] D. L. Yao, D. Siemens, V. Bernard *et al.*, JHEP **05**, 038 (2016), arXiv: 1603.03638[hep-ph]
[40] J. M. Alarcon, J. M. Camalich, and J. A. Oller, *PoS* **ConfinementX**, 122 (2012), arXiv: 1301.3067 [hep-ph]
[41] J. Alarcón, J. Martin Camalich, and J. Oller, Annals Phys. **336**, 413 (2013)
[42] A. Walker-Loud, PoS **LATTICE2013**, 013 (2014), arXiv: 1401.8259[hep-lat]
[43] M. Gong *et al.* (XQCD Collaboration), Phys. Rev. D **88**, 014503 (2013), arXiv: 1304.1194[hep-ph]
[44] M. Hoferichter, J. Ruiz de Elvira, B. Kubis *et al.*, Phys. Rept. **625**, 1 (2016)
[45] F. Alvarado and L. Alvarez-Ruso, Phys. Rev. D **105**(7), 074001 (2022), arXiv: 2112.14076[hep-ph]
[46] M. Niehus, M. Hoferichter, B. Kubis *et al.*, Phys. Rev. Lett. **126**(10), 102002 (2021), arXiv: 2009.04479[hep-ph]